ES Materials and Manufacturing
DOI: https://dx.doi.org/10.30919/esmm1127

Compensation Manipulator for Concrete 3D Printing Based on the CONPrint3D

Azamat Mustafa,[1, 2,*] Florian Storch,[3,*] Kaiyrov Rustem,[1, 5,*] Paul Plashnik,[3] Frank Will,[3] Sagyntay Mukhagali,[1, 2,*] Zhumadil Baigunchekov[4] and Volker Waurich[3]

Abstract

According to the CONPrint3D concepts, in order to improve the reliability of machine technology and expand the scope of 3D concrete printing, the printing system will be integrated into the truck-mounted concrete pump, which has the problem of insufficient positioning accuracy of the printhead. This article discusses a manipulator for compensation and positioning of the printhead from deflections of the boom of a truck-mounted concrete pump used as a construction 3D printing manipulator. The manipulator must compensate for the workspace X ±300, Y ±300, Z ±250x mm (X – length, Y – width, Z – height). To solve these problems, a comprehensive literature review of manipulators (serial, parallel, and hybrid) was carried out. Manipulators were sorted according to several criteria: degree of freedom, number of actuators, leg designs; and workspace and overall dimensions. Inverse kinematic problems are solved to determine the workspace and dimensions of the manipulators. Clavel's delta robot was selected among the manipulators, and the direct and inverse kinematics problems were solved. To understand and predict the behavior of Clavel's delta robot, a virtual experiment was made using dynamic modeling with the OpenModelica program.

Keywords: Concrete 3D printing; Manipulator; Compensating manipulator; Inverse kinematics; Direct kinematics; Dynamic simulation.
Received: 27 February 2024; Revised: 02 April 2024; Accepted: 09 April 2024.
Article type: Research article.

1. Introduction

3D concrete printing is an additive manufacturing process used to produce building structures with completely new shapes by pouring concrete into layers.[1] This has several advantages over traditional methods of construction, among them: in the construction of buildings with round or complex shapes 3D printing is faster and cheaper;[2] labor productivity is higher;[3] in the construction of single-story buildings from the economic point of view 3D printing is more profitable: in the UK by 35%,[4] in Germany by 50%,[5] in the United Arab Emirates by 78%,[6] as a raw material can use recycled concrete, environmentally efficient.[7]

Nevertheless, construction 3D printing is still a relatively new technology, and there are problems with its widespread adoption in construction, such as the cost of 3D printing equipment, the limited workspace of printing, and the need for further research and development to ensure the safety and reliability of 3D-printed structures. Most pilot projects and research work on large-scale concrete construction 3D printers based on extrusion consist of a printhead and a positioning system (manipulator). For positioning the printhead, they use a gantry,[8-14] articular,[15-19] and cable manipulators.[20,21] But these industrial robots have a limited workspace, which limits the size of printing objects, and they were originally designed for use in factories and therefore are not suitable for heavy construction site conditions.[22]

One way to increase the reliability of 3D printing designs is that traditional construction machines can be used for positioning the printhead. And so TU Dresden has developed the concept of monolithic 3D printing CONPrint3D,[23,24] which is due to the requirement of construction standards and

[1] *Department of Mechanical Engineering, Satbayev University, Almaty 050013, Republic of Kazakhstan.*
[2] *RnD center, Almaty 050067, Republic of Kazakhstan.*
[3] *Professur für Baumaschinen, TU Dresden, Dresden 01062, Germany.*
[4] *Department of Mechanics, Al–Farabi Kazakh National University, Almaty 050040, Republic of Kazakhstan.*
[5] *Laboratory of Applied Mechanics and Robotics, Karaganda Buketov University, Karaganda 100001, Republic of Kazakhstan.*
**Email:* azamat.mustafa91@gmail.com (A. Mustafa), florian.storch@tu-dresden.de (F. Storch), kairov.rustem@mail.ru (S. Mukhagali), mukhagali.sagyntay@gmail.com (S. Mukhagali)

© Engineered Science Publisher LLC 2024

aims at the maximum possible use of existing construction machinery. According to the presented concept to increase the reliability of the machine technology and to expand the scope of application the printing system is integrated into the truck-mounted concrete pump.

The truck-mounted concrete pump is used as a positioning system for the printhead. However, truck-mounted concrete pump booms are prone to mechanical deformation and vibration excitation that occur when pumping concrete[25] and rotational vibration[26] when the boom moves. To solve the above problems, an active boom vibration control strategy has been proposed,[27-31] and X. Sun *et al*. proposed a closed-loop detection and open-loop control strategy communication to track the trajectory.[32] Cazzulani *et al*. considered a truck-mounted concrete pump as two subsystems: the boom and the truck-mounted concrete, they studied the effect of boom vibration exerted by each subsystem, and research achievements provide a theoretical basis for the control of boom vibration.[33] However, these works only consider boom vibration without taking into account fluctuations due to boom deformation. In the work of S. Zorn *et al*.,[34] a simulation model of a truck-mounted concrete pump boom was created, which, in addition to the movements of the boom segments relative to each other, also takes into account the steel deformations of the boom segments and the behavior of the hydraulic cylinders. Although this work indicates that the work is important for adapting a truck-mounted concrete pump to work as a construction 3D printer, it does not provide specific values for the minimum and maximum deviations. In the work,[35] which is a logical continuation of this work, the deviation from the specified trajectory on average along the axes is indicated: X 90 mm, Y 51 mm, z 150 mm. Such accuracy of positioning is not acceptable for 3D printing with concrete. The positioning accuracy of the printhead must comply with the design tolerances of DIN 18202.

To compensate for boom deflections and to increase printing accuracy by DIN 1study and design of the manipulators are required.

2. Methods

2.1 Formulation of the problem

The manipulator for the compensation unit used in the 3D printing process must be compact and lightweight in order not to impair the dynamic properties of the printhead positioning system. It must also have good dynamic performance, which is necessary to realize fast compensating movements.[36-37] The required degrees of freedom of the compensating unit must be determined depending on the motion system of the printhead (in our case, the movement of the truck-mounted concrete pump boom) and the planned printing trajectory. Fig. 1 shows the procedure for printing a wall in a straight line using a truck-mounted concrete pump.

The truck-mounted concrete pump is located in the global coordinate system *B*. The boom of the truck-mounted concrete pump moves in the cylindrical coordinate system and has 3 DOF: rotational along the axis Z_M and movement along the axes $Y_M Z_M$. The concrete layer to be printed is described in the *S* coordinate system and is also located in the coordinate system *B*. The *D* coordinate system represents the printhead.

The truck-mounted concrete pump links work as a planar sequential manipulator. To print a wall along a straight path (coordinate system *S*), it is necessary that the printhead (axis - Z_D) always remains in a vertical position relative to the plane of the printed wall (axis - $X_S Y_S$), thus, the $X_D Y_D$plane and the $X_S Y_S$ plane of the layer needs to be parallel. The vertical position of the printhead is controlled by the rotational movement (axis - X_D) between the connection of the last boom of the truck-mounted concrete pump and the printhead. To follow the orientation of the wall (e.g. if the wall has a 90° corner) during the printing process, it is necessary to rotate the printhead around the Z_D axis. And at the end, translational deviations along the axes X_D, Y_D and Z_D are compensated.

As you know, large weight compensation will require a correspondingly large manipulator with large power and

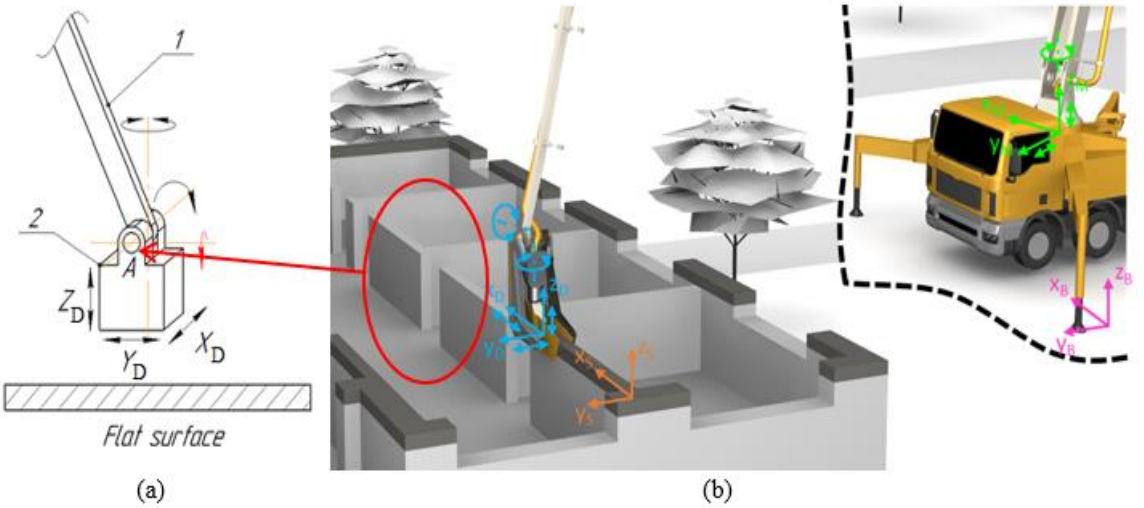

Fig. 1 Determination of the necessary movements for precise positioning during the printing process (a) DOF compensation unit, 1 – last boom, 2 – printhead (b) world frame compensation block.

 © Engineered Science Publisher LLC 2024

dimensions. To simplify compensation tasks, the compensation unit can be divided into two parts: a) mechanism for keeping the printhead in the vertical position and b) compensation of translational deviations of the nozzle along the *XYZ* axes (Fig. 2). The rotation along the *Z* axis to change the trajectory of the printing wall was provided when designing the nozzle, that is, the nozzle is rotated by an independent motor separately (nozzle rotation[38]).

The vertical position of the printhead is ensured by the Watt or Stephenson lever mechanism. To compensate for the translation movement deflection we need to choose a suitable manipulator and for this, we have sorted the manipulators in section 2.2.

Based on traditional construction standards and the results of TU Dresden's research,[39-42] a basic requirement for a compensation manipulator was drawn up. Which includes: compensation workspace - $X \pm 300$, $Y \pm 300$, $Z \pm 250$ mm is the deviation of the last boom of the truck-mounted concrete pump which was determined by research work at the Technical University Dresden;[39-42] the maximum moving speed of the manipulator is 0.2 m/s, which is the printing speed; [36] the positioning accuracy of ±5 mm was determined by the tolerances of the building design according to DIN 18202; and finally the degree of protection IP65 and above which are designed to protect against aggressive conditions like dust, dirt, and water.

2.2 Sorting manipulators for the nozzle to compensate for translation movements

2.2.1 Comparison of manipulators

When choosing suitable kinematics, in addition to the DOF, dynamic and structural aspects must also be considered. Typical dynamic issues are load capacity, posture-dependent system stiffness, or acceleration capability.

To select a manipulator that meets the above requirements, a deep literary analysis of manipulators was made: serial and parallel structures (Table 1).

A serial manipulator is a chain mechanism connecting several joints in various ways (usually rotating and prismatic). Serial manipulators are also called open-chain manipulators because one end of the manipulator is attached to the fixed base, while the other end (end-effector) is free to move in space.[43]

The parallel manipulator is a mechanical system consisting of two connected platforms, namely a fixed platform and a moving platform, connected by at least two independent legs. Compared to serial analogs, parallel manipulators consist of closed kinematic chains.[44]

Table 1. Comparison table of serial and parallel manipulators.

Characteristics[45]	Serial manipulator 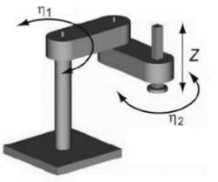	Parallel manipulator 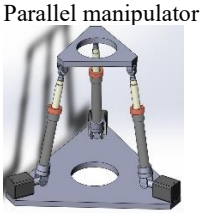
Structural rigidity	Low	High
Manipulator weight	Big	Small
Load capacity	Low	High
Inertial load	High	Low
Positioning accuracy	Low	High
Workspace	Big	Small
Work and installation space	Big	Small

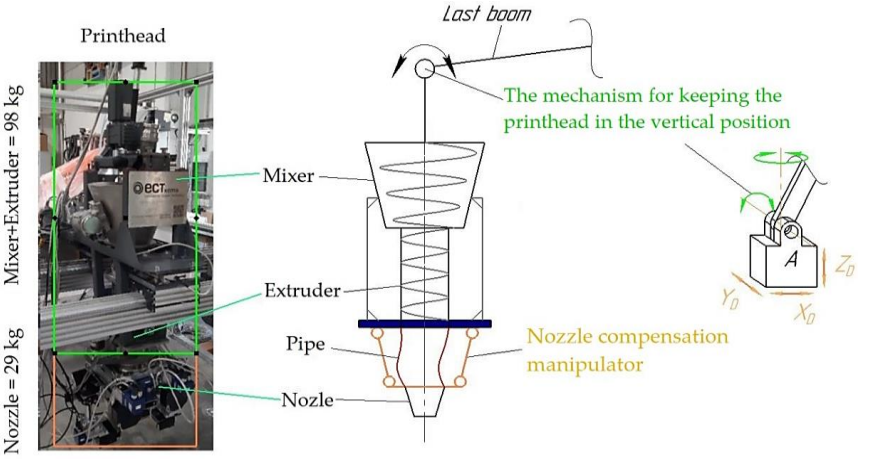

Fig. 2 PrintHead and installation options for the mechanism for keeping the PrintHead in the vertical position and nozzle compensation manipulator.

© Engineered Science Publisher LLC 2024

Some properties of the manipulator types are compared in Table 1. Serial manipulators have some advantages: they have a large workspace and can be skillfully maneuvered. However, due to the cantilever construction, their load capacity is limited.[46] The work of Reimund Neugebauer,[47] Uchiyama M. D,[48] or Hesse Stefan and Malisa Viktorio[49] essentially emphasizes the lower moving mass and the more favorable dynamic properties of parallel robots compared to serial manipulators but they often have a limited workspace. A hybrid manipulator is a combination of closed and open chain mechanisms or serial-parallel mechanisms. These manipulators try to overcome the limited workspace of parallel manipulators and provide functions of both sequential and parallel manipulators.[50-52]

Since serial manipulators do not meet the set requirements such as structural rigidity, high load capacity, high positioning accuracy with high-speed end-effector movements, and the ratio of mass to load capacity, that is why serial manipulators are excluded from the candidates for the compensation manipulator. Next, parallel and hybrid manipulators are considered.

The manipulator is sorted into two steps, in the first step section 2.2.1.: by DOF, number of drives, and leg design. In the second step section 2.2.2: workspace and dimensions. The workspace of the manipulators must be $X = \pm 300$, $Y \pm 300$, $Z = \pm 250$ mm (length - X; width - Y; height - Z).

2.2.2 Sorting manipulators by DOF and leg structure

The first criterion to select a manipulator for the compensation of the translational movements is the number of DOF of the entire manipulator. Parallel and hybrid manipulators have translational, rotational, or mixed DOF.[53] For choosing a manipulator, it's important to reduce the structure to the necessary DOF. This will also reduce the number of drivers and in the end, the total mass of the manipulator, and this improves the movements with the boom of the truck-mounted concrete pump.

According to the literature review, the main types of parallel manipulators were distinguished, and they can be divided by the structures (by the number of legs from 3-6) (Fig. 3).

3-leg parallel manipulators, also called tripods, have three legs connected to the platforms via joints. There are many different leg structures to realize only rotational or mixed 3 DOF, e.g. 3-UPS,[54] 3-RPS,[55] 3-RPU,[56] 3-PRS.[57,58] It's also possible to move 6 DOFs with Tripods if several joint DOFs are driven in the individual leg chains, for example, 3-RRRS[59] which is driven by six rotating joints or 3SPU,[60] and redundantly actuated 3UPS PMs.[61] In the context of this publication, tripods with purely translational movements are

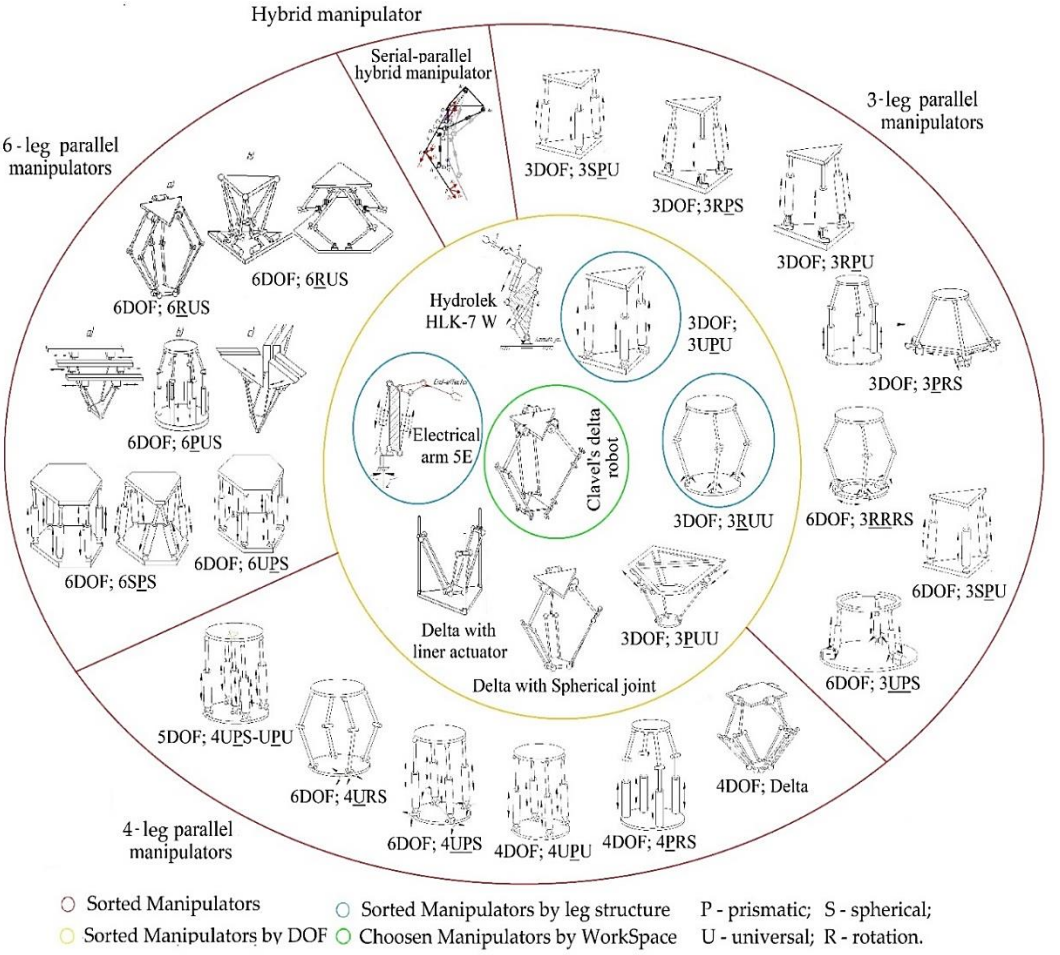

Fig. 3 Sorted manipulators of parallel and hybrid structures.

 © Engineered Science Publisher LLC 2024

more interesting, for example (in the yellow circle): 3-UPU by Tsai or Hassani,[62,63] 3-RUU by Bałchanowski,[64] 3-PUU by Li and Xu,[65] and Calvel's delta robot (3-RRR).[66] Based on the 3-RRR, other similar structures have been developed, which are essentially different in the joint types used and the respective driven joint of the chain. Examples of these leg structures are 3-RUU[67] or 3-PUU.[68]

The extension of the number of legs usually results in the way, that the number of DOFs increases in the same way. As an example, the 4-legged delta robot,[69] the 4-PRS,[70] or 4-UPU,[71,72] have either one more translational or rotational degree of freedom. As with tripods, 6 DOF can also be realized with 4-legged manipulators, *e.g.* 4-UPS[73] or 4-URS.[74] In the 4-UPS-UPU add two different legs and the final manipulator has 5 DOF.[75]

The best-known 6-leg parallel manipulator is the Stewart-Gough platform (6-SPS).[76,77] This can alternatively also be designed with the 6-UPS leg structure.[78] A similar structure of kinematics can be achieved if the order of the joints is exchanged within the closed kinematic chain, e.g. 6-PUS.[79,80] Some variations to avoid translational joints are shown by the structure 6-RUS.[81,82] All the manipulators presented have 6 degrees of freedom.

The hybrid manipulators (serial-parallel structure) shown in Fig. 3 have a serial structure: serial-parallel hybrid manipulator,[83] Hydrolek HLK-7 W[84] and Electrical arm 5E[85] (in the yellow circle). One driver allows rotation around the *Z*-axis and the other drives are combined in corresponding parallel kinematic mechanisms to realize the plane movement in the arm plate and increase the system stiffness.

As shown in Fig. 3, only the parallel kinematic manipulators that perform purely translational DOF are selected for closer examination, which means (in the yellow circle): 3-UPU; 3-RUU; 3-RRR; 3-RSS, and 3-PUU. Among the hybrid manipulators with mixed DOF, the Serial-Parallel structure Hydrolek HLK-7 W and the Electrical arm 5E are shortlisted, because hybrid manipulators possess the advantages of both serial and parallel manipulators from a rigidity and workspace point of view.[86,87]

The next selection criterion is the type of joints within the kinematic chains. These joints influence to a considerable extent the size of the workspace, the manipulability within the workspace, the positioning accuracy due to bearing play, the system rigidity, or the manufacturing costs. The selected manipulators have a large number of rotatable, spherical, or universal joints in non-driven joints. Neugebauer[47] describes the advantages and disadvantages of those joint types. It is determined that swivel and cardan joints have a higher stiffness and load capacity compared to ball joints. Therefore, manipulators that have spherical joints are not considered further. Methods determining the workspace and preliminary dimensions are made for the following manipulators: 3-UPU; 3-RRR (Clavel's Delta Robot); 3-RUU; Electrical arm 5E (in the paragraph 2.2.3).

2.2.3 Sorting of manipulators by workspace and dimensions

In the second step, the manipulators are sorted by workspace and dimensions. To find the workspace and overall dimensions, it is necessary to solve the inverse kinematics problems of the manipulators. Inverse kinematics is the determination of the joint angles of a manipulator required to position its end effector at a specific pose in space. After solving the inverse kinematic problem, the workspace (X ±300, Y ±300, Z ±250 mm) is determined in MatLab software. Analyzing the workspace can help determine optimal design parameters, such as link lengths and joint configurations.

Inverse kinematics problems were solved for the sorted manipulators. For the 3-UPU manipulator look Hamida.[88] Tsai[89] solved the inverse kinematics of the delta robot (3-RRR) by using the Denavit-Hartenberg method. Bałchanowski[64] formulates the inverse kinematic problem of the 3-RUU manipulator in his work. The electric arm 5E (hybrid manipulator) has the structure R(RPRR)+R(RPR). The linear actuators move the mechanism along the XY axes and rotate along the *Z*-axis. Since the manipulator is based on an articulated manipulator, its workspace is determined based on a two-link serial manipulator according to the method of Zar T., Lin P.W[90] and the rotation around the *Z*-axis is added afterward. Using the methods of the above authors, the inverse kinematics problems were solved and the workspaces of the manipulators were determined (the results are shown in paragraph 3.1).

2.3 Geometry and mobility

The nozzle compensation manipulator (hereinafter referred to as Clavel's delta robot) consists of a moving platform 5 connected to a fixed platform 1 by identical three kinematic chains $A_i, C_i, D_i (i = 1,2,3)$. Each chain contains rotational connections A_i, driven by drive 2 on the fixed platform 1. The movement is transmitted to the movable platform through parallelograms whose centers are points $C_i$and D_i formed by links and hinges (Fig. 4). Such a robot has a positioning accuracy of about 0.1 mm.[91]

2.4 Inverse kinematics

Let's make the equations of closed leg contours

$$r_{D_i} = r_{OP} + h_i, (i = 1,2,3). \quad (1)$$

The components of the vectors r_{D_i} through the PM leg parameters, using the homogeneous Denavit-Hartenberg transformation matrices[77] are defined as follows:

$$X_{D_i} = r_a \cdot cos\theta_i + L_2 \cdot cos\varphi_{1i} \cdot cos\theta_i + L_1 \cdot sin\varphi_{3i} \cdot sin\theta_i + L_1 \cdot cos\varphi_{3i} \cdot cos\theta_i \cdot cos(\varphi_{1i} + \varphi_{2i}),$$

$$Y_{D_i} = r_a \cdot sin\theta_i + L_2 \cdot cos\varphi_{1i} \cdot sin\theta_i - L_1 \cdot cos\theta_i \cdot sin\varphi_{3i} + L_1 \cdot cos\varphi_{3i} \cdot sin\theta_i \cdot cos(\varphi_{1i} + \varphi_{2i})$$

$$Z_{D_i} = L_2 \cdot sin\varphi_{1i} + L_1 \cdot cos\varphi_{3i} \cdot sin(\varphi_{1i} + \varphi_{2i}). \quad (2)$$

© Engineered Science Publisher LLC 2024

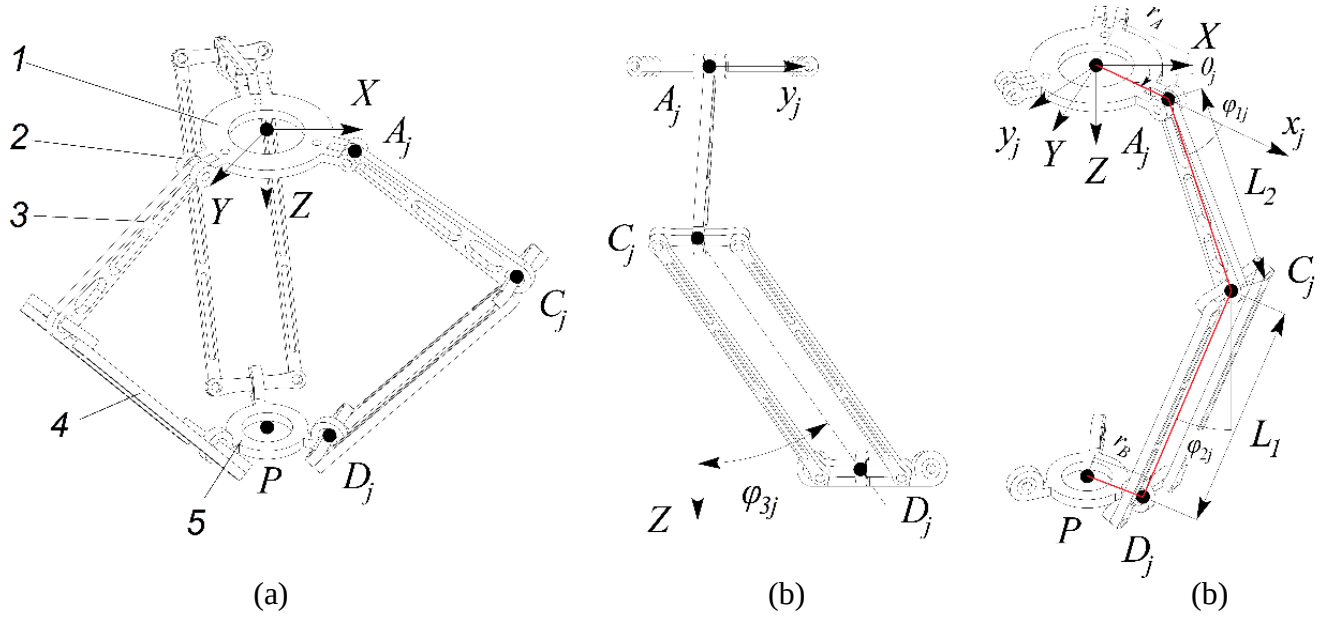

(a) (b) (b)

Fig. 4 Clavel's Delta robot structure: (a) main view, (b) considering one leg separately, and (c) Clavel's Delta robot parameters.

When solving the inverse kinematics problem, we set the position and orientation of the moving platform, and determine the hinge angles that determine the configuration of each leg $\varphi_{1,i}, \varphi_{2,i}, \varphi_{3,i} (i = 1,2,3)$, for the right side of equations (1)

$$\begin{bmatrix} X_{D_i} \\ Y_{D_i} \\ Z_{D_i} \\ 1 \end{bmatrix} = \begin{bmatrix} 1 & 0 & 0 & X_P \\ 0 & 1 & 0 & Y_P \\ 0 & 0 & 1 & Z_P \\ 0 & 0 & 0 & 0 \end{bmatrix} \begin{bmatrix} r_b \cdot cos\theta_i \\ r_b \cdot sin\theta_i \\ 0 \\ 1 \end{bmatrix}, i = 1,2,3, \quad (3)$$

where $\theta_1 = 0, \theta_2 = \frac{2\pi}{3}, \theta_3 = \frac{-2\pi}{3}$.

From equality (3) we obtain

$$X_{D_i} = X_P + r_b \cdot cos\varphi_i, Y_{D_i} = Y_P + r_b \cdot sin\varphi_i, Z_{D_i} = Z_P, i = 1,2,3. \quad (4)$$

From equations (2) and (4) we obtain the coordinates of the center of the local coordinate system $O_P X_P Y_P Z_P$

$$X_P = r \cdot cos\theta_1 + L_2 \cdot cos\varphi_{11} \cdot cos\theta_1 + L_1 \cdot sin\varphi_{31} \cdot sin\theta_1 + L_1 \cdot cos(\varphi_{11} + \varphi_{21}) \cdot cos\varphi_{31} \cdot cos\theta_1, \quad (5)$$

$$Y_P = r \cdot sin\theta_1 + L_2 \cdot cos\varphi_{11} \cdot sin\theta_1 - L_1 \cdot cos\theta_1 \cdot sin\varphi_{31} + L_1 \cdot cos(\varphi_{11} + \varphi_{21}) \cdot cos\varphi_{31} \cdot sin\theta_1, \quad (6)$$

$$Z_P = L_2 \cdot sin\varphi_{11} + L_1 \cdot sin(\varphi_{11} + \varphi_{21}) \cdot cos\varphi_{31}, \quad (7)$$

where $r = r_a - r_b$.

From the sum of squares of equations (5), (5) and (7) we obtain

$$(X_P - X_i)^2 + (Y_P - Y_i)^2 + (Z_P - Z_i)^2 - L_1^2 = 0, \quad (8)$$

where $x_i = \cos\theta_i \cdot (r + L_2 \cdot cos\varphi_{1i}), y_i = \sin\theta_i \cdot (r + L_2 \cdot cos\varphi_{1i}), z_i = L_2 \cdot sin\varphi_{1i}, i = 1,2,3$.

By opening the brackets of equation (8) we give the following form

$$l_1 \cdot \cos\varphi_{1i} + m_1 \cdot \sin\varphi_{1i} - n_1 = 0 \quad (9)$$

where $l_i = 2 \cdot r \cdot L_2 - 2 \cdot L_2 \cdot X_P \cdot cos\theta_i - 2 \cdot L_2 \cdot Y_P \cdot sin\theta_i, m_i = -2 \cdot L_2 \cdot Z_P, n_i = -(r^2 - L_1^2 + X_P^2 + Y_P^2 + Z_P^2 - 2 \cdot X_P \cdot r \cdot cos\theta_i - 2 \cdot Y_P \cdot r \cdot sin\theta_i + L_2^2)$.

Solved equation (9) and obtain two solutions corresponding to two assemblies of each leg of the PM

$$\varphi_{1i1} = acos(n_1/k_1) + \alpha_1 and \varphi_{1i2} = -acos(n_1/k_1) + \alpha_1, \quad (10)$$

s

where $k_1 = \sqrt{l_1^2 + m_1^2}, \alpha_1 = atan(m_1/l_1)$.

From the addition of (5) and (6) equations, previously multiplying (5)-equation by $cos\theta_j$, (7)-equation $sin\theta_j (j = 1,2,3)$ we get

$$L_1 \cdot cos\varphi_{3i} \cdot cos\varphi_{12i} = a, \quad (11)$$

where $a = (X_P - (r + L_2 . cos\theta_{1i}) \cdot cos\theta_1 + (Y_P - (r + L_2 \cdot cos\varphi_{1i}) \cdot sin\theta_1) \cdot sin\theta_1, \varphi_{12i} = \varphi_{1i} + \varphi_{2i}$.

(7) - the equation is reduced to the following form

$$L_1 \cdot cos\varphi_{3i} \cdot sin\varphi_{12i} = b, \quad (12)$$

where $b = Z_P - L_2 \cdot sin\varphi_{1i}$.

From the (12)-equation on (11) we obtain

$$\varphi_{2j} = atan(b/a) - \varphi_{1j}. \quad (13)$$

Adding the squares of equations (11) and (12) we get

$$\varphi_{3j} = \pm acos\sqrt{(a_j^2 + b_j^2)/L_1^2}. \quad (14)$$

The sign before φ_{3j} in equation (14) will change depending on the signs of X_P and Y_P.

2.5 Direct kinematics

To solve the direct kinematics problem of Clavel's delta robot, the positions of active revolute kinematic pairs φ_{1j} are specified and the coordinates of the center of the moving platform X_P, Y_P, Z_P are determined, respectively the rotation angles of the passive revolute kinematic pairs $\varphi_{2j}, \varphi_{3j}$ and the position of the parallel robot links are determined.

Equations (8) are reduced to the following form

$$\left.\begin{aligned} (X_P - X_1)^2 + (Y_P - Y_1)^2 + (Z_P - Z_1)^2 - L_1^2 = 0 \\ (X_P - X_2)^2 + (Y_P - Y_2)^2 + (Z_P - Z_2)^2 - L_1^2 = 0 \\ (X_P - X_3)^2 + (Y_P - Y_3)^2 + (Z_P - Z_3)^2 - L_1^2 = 0 \end{aligned}\right\}. \quad (15)$$

 © Engineered Science Publisher LLC 2024

By opening brackets from the first equation of the system (15) we take away the second equation and from the first equation we take away the third equation and we get the following two equations

$$\left.\begin{aligned} m_{11}\cdot X_P + m_{12}\cdot Y_P + m_{13} - 2\cdot Z_P\cdot Z_1 + 2\cdot Z_P\cdot Z_2 = b_1 \\ m_{21}\cdot X_P + m_{22}\cdot Y_P + m_{23} - 2\cdot Z_P\cdot Z_2 + 2\cdot Z_P\cdot Z_3 = b_2 \end{aligned}\right\}, \quad (16)$$

where $m_{11} = -2\cdot X_1 + 2\cdot X_2, m_{12} = -2\cdot Y_1 + 2\cdot Y_2$, $m_{13} = X_1^2 + Y_1^2 + Z_1^2 - X_2^2 - Y_2^2 - Z_2^2$, $m_{21} = -2\cdot X_2 + 2\cdot X_3, m_{22} = -2\cdot Y_2 + 2\cdot Y_3, m_{23} = X_2^2 - X_3^2 + Y_2^2 - Y_3^2 - Y_3^2 + Z_2^2$.

Equations (16) are written in matrix form

$$A\cdot\begin{bmatrix} X_P \\ Y_P \end{bmatrix} = B, \quad (17)$$

where $A = \begin{pmatrix} m_{11} & m_{12} \\ m_{21} & m_{22} \end{pmatrix}, B = \begin{pmatrix} -m_{13} + 2\cdot Z_P\cdot Z_1 - 2\cdot Z_P\cdot Z_2 \\ -m_{23} + 2\cdot Z_P\cdot Z_2 - 2\cdot Z_P\cdot Z_3 \end{pmatrix}$.

From equation (16) we find X_P and Y_P as follows

$$X_P = (k_{11}\cdot Z_P + k_{12}), Y_P = (t_{11}\cdot Z_P + t_{12}), \quad (18)$$

From the third equation of the system (15), taking into account equation (18), we obtain where $k_{11} = 2\cdot(-m_{12}\cdot Z_2 + m_{12}\cdot Z_3 + m_{22}\cdot Z_1 - m_{22}\cdot Z_2)/q, k_{12} = (m_{12}\cdot m_{23} - m_{13}\cdot m_{22})/q$, $t_{11} = 2\cdot(m_{11}\cdot Z_2 - m_{11}\cdot Z_3 - m_{21}\cdot Z_1 + m_{21}\cdot Z_2)/q, t_{12} = (m_{13}\cdot m_{21} - m_{11}\cdot m_{23})/q$, $q = m_{11}\cdot m_{22} - m_{12}\cdot m_{21}$.

From the third equation of the system (15), taking into account equation (18), we obtain

$$Z_P = \frac{-2\cdot(k_{11}\cdot k_{12} - k_{11}\cdot x_3 + t_{11}\cdot t_{12} - t_{11}\cdot y_3 - z_3) \pm \sqrt{D}}{2\cdot(k_{11}^2 + t_{11}^2 + 1)}, \quad (20)$$

where $D = (2\cdot k_{11}\cdot k_{12} - 2\cdot k_{11}\cdot X_3 + 2\cdot t_{11}\cdot t_{12} - 2\cdot t_{11}\cdot Y_3 - 2\cdot Z_3)^2 - -4\cdot(k_{11}^2 + 1 + t_{11}^2)\cdot(k_{12}^2 - 2\cdot k_{12}\cdot X_3 + t_{12}^2 - 2\cdot t_{12}\cdot y_3 + X_3^2 + Y_3^2 + Z_3^2 - L_1^2)$.

From equation (18) taking into account (19) we obtain values X_P and Y_P. Thus, using the direct kinematics problem we check the inverse problem.

2.6 Dynamic simulation

The dynamic simulation of Clavel's delta robot is based on the multibody system approach. To simulate the dynamic behavior of the Clavel's delta robot (dynamic simulation), the OpenModelica program was used, which provides a comprehensive modeling and simulation platform for multi-body systems (Fig. 5) (the operating principles and kinematics of Clavel's delta robot are described in chapter "2.3. Geometry and mobility"). This includes modeling the mechanical structure actuators, and sensors of Clavel's delta robot. This model takes into account the physical properties of the robot components such as mass, length, and moments of inertia and enable the movement behavior.[92] Sensors can be used to measure various parameters such as the position, speed, and acceleration of robot components. The model was constructed utilizing OpenModelica library joints, which account DOF.

To do this, first, the mechanical structure of Clavel's delta robot is built using - Modelica.Mechanics.MultiBody (Fig. 5). Where is shown world reference (1), fixed platform where are axis1, axis2, axis3 (2), 3 similar legs structure (3) and moving platform (4). The world reference model (1) establishes both the inertial reference frame and the gravitational field, which is a constant requirement when employing the MultiBody package.[93] The fixed platform (2) and the moving platform (4) can have different shapes, however, dynamics is only defined by the inertial parameters of a single rigid body; in this case, fixed and moving platforms have been modeled as cylinders. The upper arm rotational joints are attached to the fixed

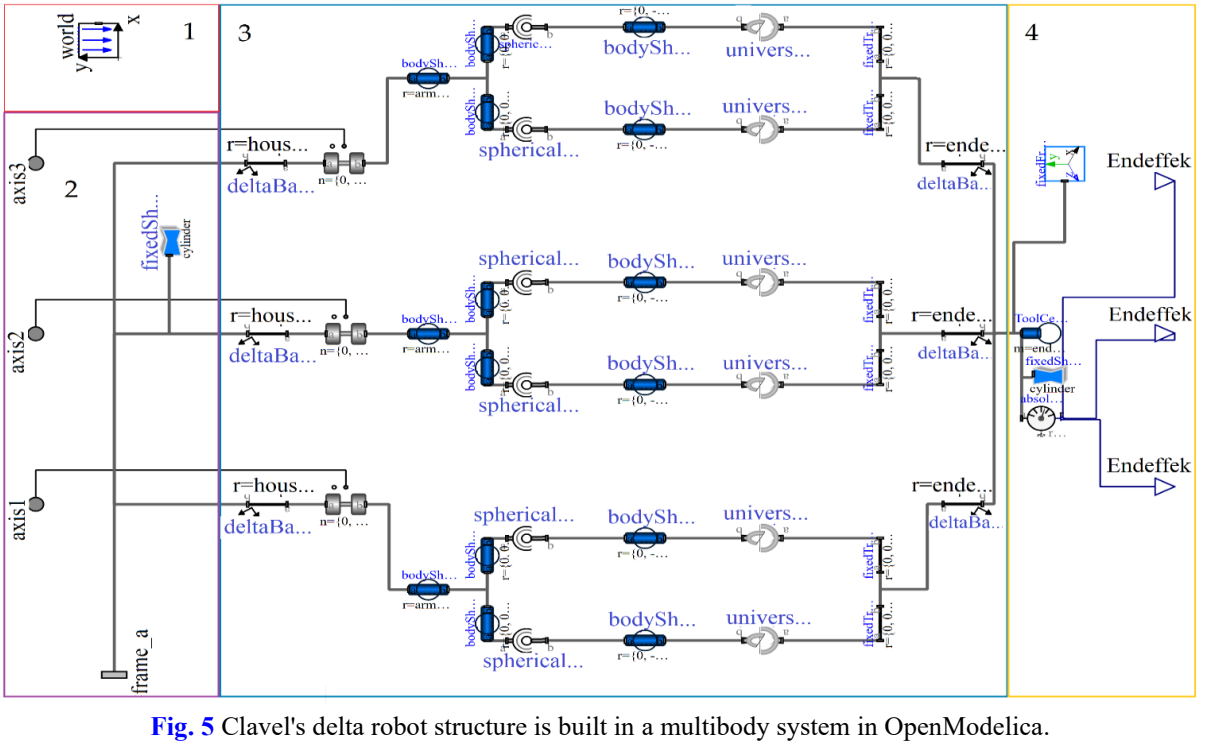

Fig. 5 Clavel's delta robot structure is built in a multibody system in OpenModelica.

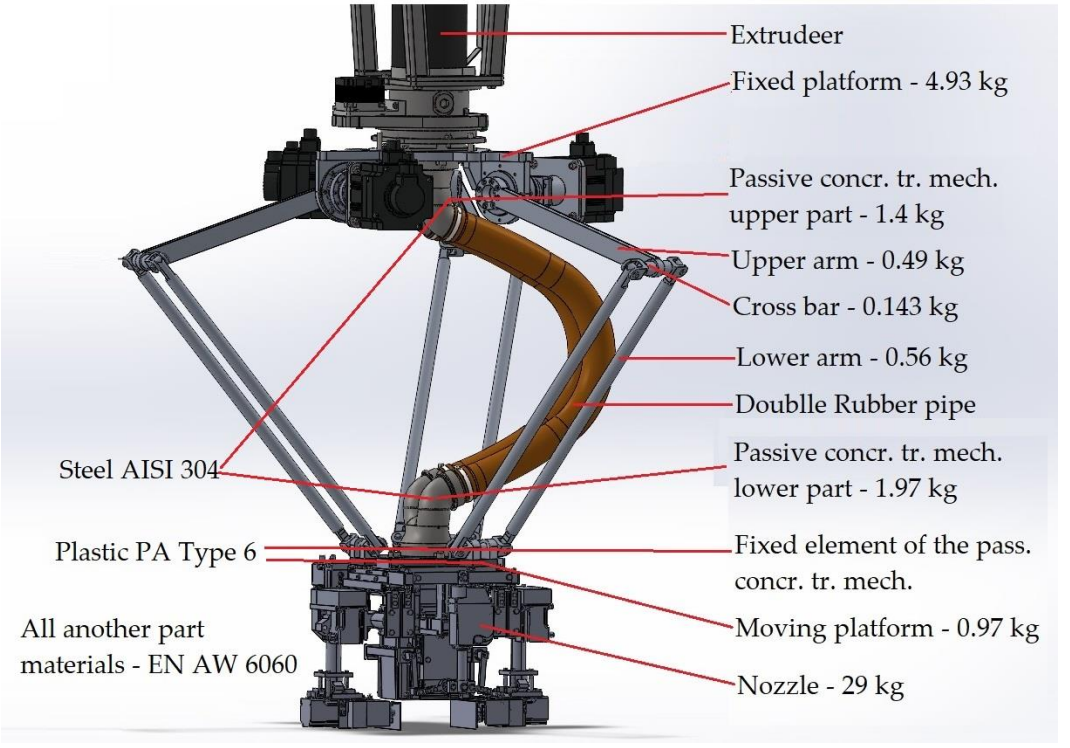

Fig. 6 3D model of the Clavel's delta robot and structural elements masses.

platform, and parallelograms are attached to the moving platform (3), they are located 120 degrees relative to each other.

To enter the mass data of the structural elements of Clavel's delta robot, a 3D model of Clavel's Delta robot was modeled in SolidWorks (Fig. 6). The materials were selected taking into account the strength and weight of the material, as well as construction site conditions, the main of which is resistant to corrosion. The material of the moving platform and the fixed element of the passive concrete transport mechanism is plastic PA Type 6. And the material of the passive concrete transport mechanism's pipe is steel AISI 304. The material of all other elements is aluminum EN AW 6060. Fig. 6 shows the weights of the structural elements of Clavel's delta robot. Summing up the masses of the nozzle, passive concrete transporting mechanism, and concrete (inside mechanisms) the mass for compensation is 46 kg.

After that, in the Robot Parameters block (Fig. 7), the masses of the links and the dimensions of Clavel's delta robot are entered as input data.

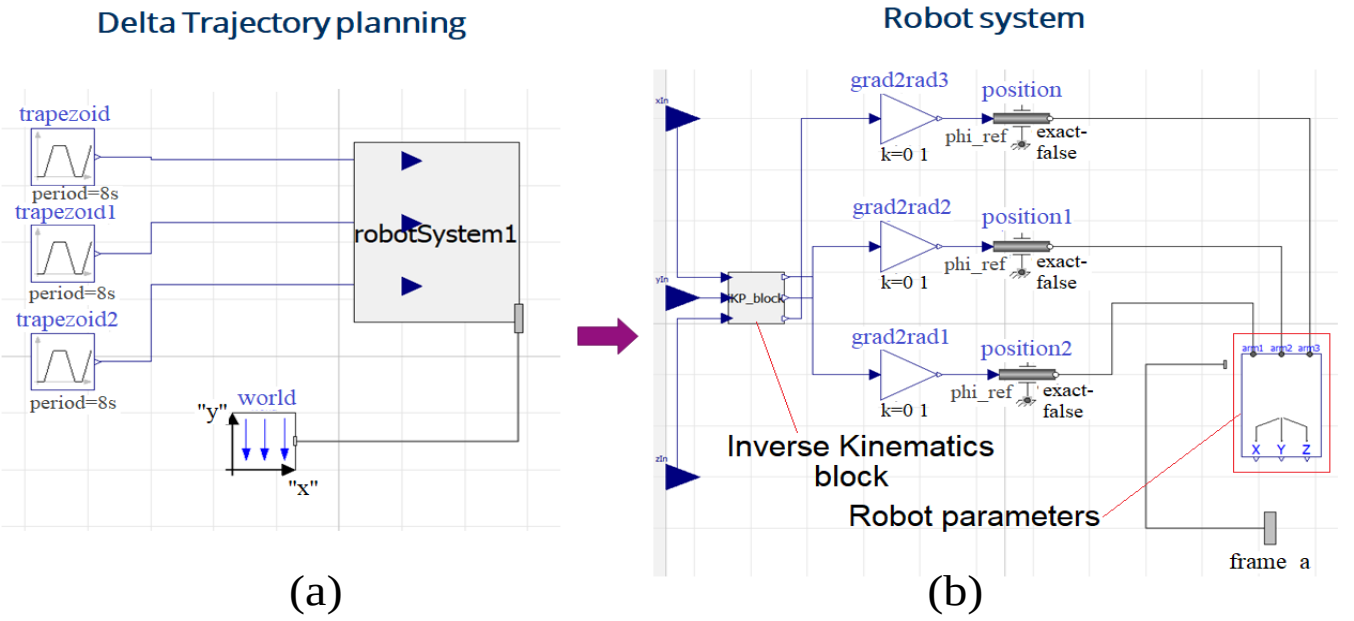

Fig. 7 Block diagrams: (a) a path planar and (b) a position-based control.

 © Engineered Science Publisher LLC 2024

The Delta Trajectory planning block (Fig. 7a) outlines the path taken by the origin of the platform reference moving platform. Currently, it supports linear, trapezoidal, and cubic trajectories, which are subject to validation. The movement of the end-effector is carried out with the Robot System block (Fig. 7b) using inverse kinematics equations to determine the articulation angles to calculate reference signals for the motor coordinate controllers. Trajectory, mass, and articulation angle data are used to determine the acceleration and torque required for each motors.

In order to determine the maximum loaded position of Clavel's delta robot 6 positions of the moving platform are identified (Fig. 8), which three middle positions - P1, P2, P3 and three extreme positions - P4, P5, P6. The trajectory of the moving platform is set with the help of the Delta Trajectory planning unit. The maximum speed of the platform movement is 0.2 m/s, acceleration 0.6 m/s² and the moving mass is 46 kg.

3. Results and discussion

3.1 The sorting results of manipulators by workspace and dimensions

The workspace results for 3-UPU; 3-RRR (Clavel's delta robot), 3-RUU, and the 5E electric arm are summarized in Table 2. The needed workspace are X ± 300, Y ± 300, and Z ± 250 × mm (X – length, Y – width, Z – height). The optimal lengths of the manipulator links were also determined following the working area. As shown in Table 2, the 3RUU manipulator has an upper leg size of 550 mm and a lower leg of 950 mm, and the 3UPU manipulator has a rod body size of 880 mm and a rod size of 700 mm, which exceeds the overall dimensions of the 3-RRR (Clavel's Delta Robot) and Electrical arm manipulators.

Thus, when comparing manipulators for compensation nozzle, Clavel's Delta Robot (3-RRR) and the "Electric arm" stand out, as they are compact and have a good ratio of the workspace to the size of the structures, see Table 2. Clavel's delta robot is seen as the preferred option as it can perform very fast and precise movements.[94,95] Also, the parallel structure of the manipulator makes it possible to achieve sufficient rigidity of the system in all positions due to the closed kinematics.[96] Another reason for choosing is the simple design and lightweight.

3.2 The inverse kinematics results

The following constant parameters were set: $r_a = 182.5, r_b = 105, r = r_a - r_b, L_1 = 740,\ L_2 = 440, \theta_1 = 0, \theta_1 = 0^0, \theta_2 = 120^0, \theta_3 = 240^0$ and also the coordinates of the moving platform center: $X_P = 300,\ Y_P = 300,\ Z_P = 250$. Fig. 9 shows Clavel's delta robot position of the robot for specific numerical values. A program was made that automatically changes the solutions of the equations depending on the signs of the coordinates of the center of the mobile platform and determines the position.

If the coordinates of the center of the moving platform X_P, Y_P, Z_P are set, for example, X_P, Y_P from -500 to +500 with step 50, and Z_P from 450 to 1100 with step 50 (Fig. 10) you can get the workspace of the parallel robot based on the inverse kinematics problem.

Table 2. Comparison of the workspace of the manipulators for the nozzle compensation.

Type	Parallel			Hybrid
Kinematic structure	3-RRR (Clavel's Delta Robot)	3RUU	3UPU	R(RPR)+R(RPR) (Electrical arm)
Dimensions	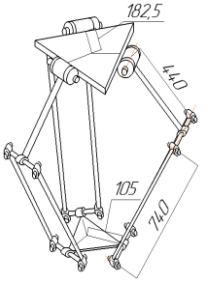	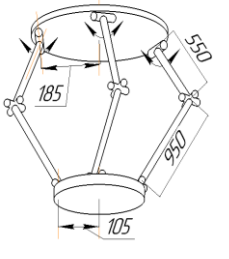	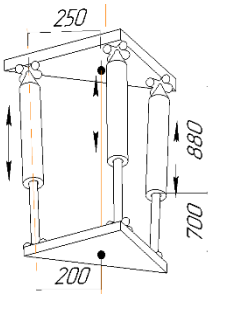	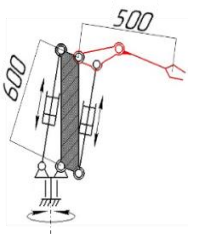
Workspace	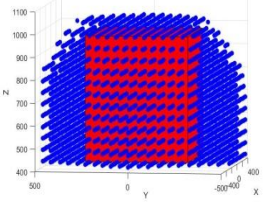	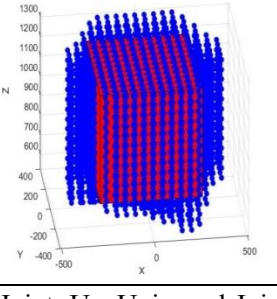	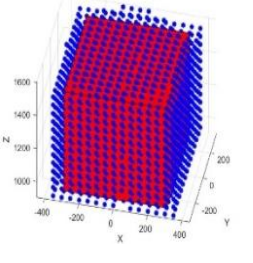	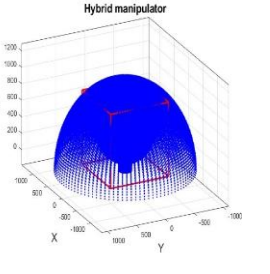

Legende: P - Prismatic Joint; R - Rotation Joint; U - Universal Joint; driven joint Blue dots - manipulator workspace; Red cube - necessary workspace.

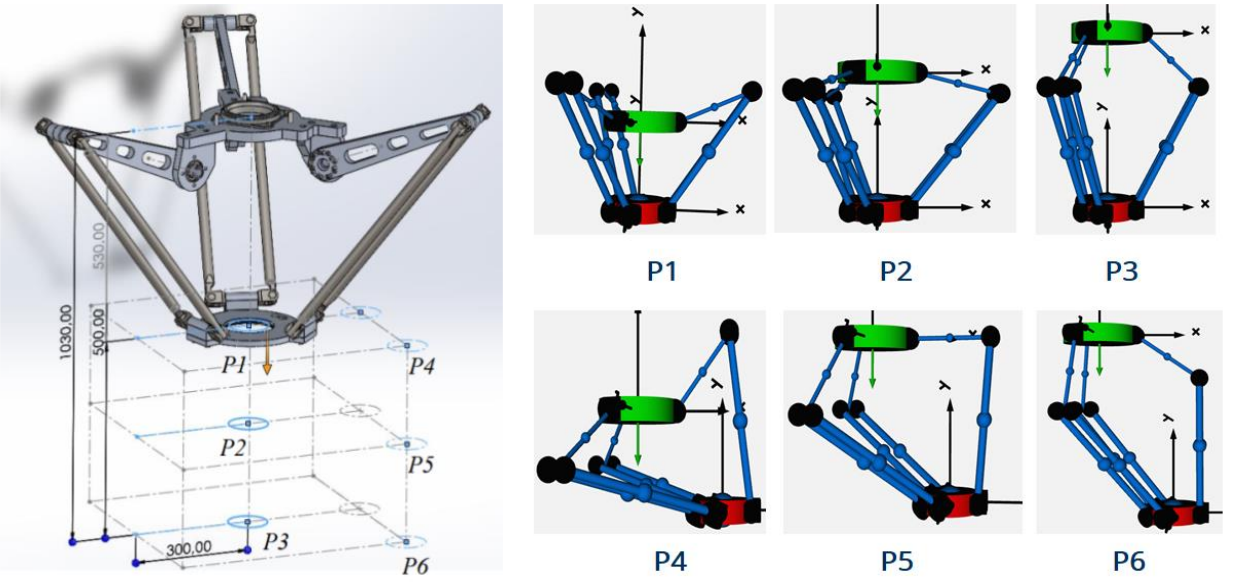

Fig. 8 6 position of Clavel's delta robot.

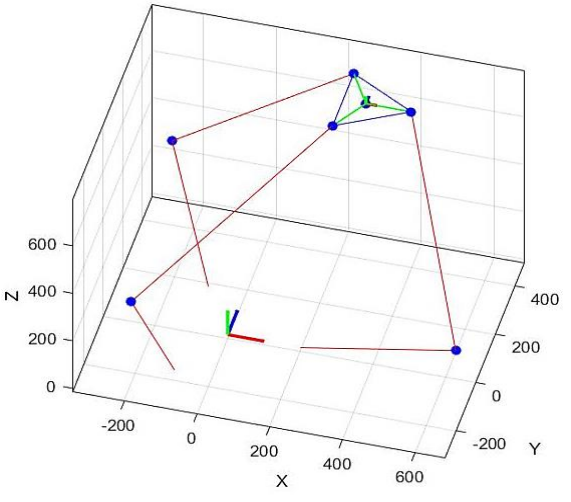

Fig. 9 Solution of the inverse kinematics problem.

As shown in Fig. 10, the defined workspace of Clavel's delta robot based on the inverse kinematics problem shows that it can provide a workspace of $X_P = 300,\ Y_P = 300,\ Z_P = 250$.

3.3 The direct kinematics results

We set the following constant parameters $r_a = 182.5, r_b = 105, r = r_a - r_b, L_1 = 740,\ L_2 = 440, \theta_1 = 0, \theta_1 = 0^0, \theta_2 = 120^0, \theta_3 = 240^0$. The rotation angles of active kinematic pairs are set from the values obtained by the inverse kinematics problem $\varphi_{11} = 0.2398, \varphi_{12} = 0.5620, \varphi_{13} = 1.1922$. The obtained coordinates of the centers of the moving platform of the parallel manipulator coincide with the values of the inverse kinematics problem.

3.4 The dynamic simulation results

This paragraph shows the results of dynamic simulations to determine the maximum load state for Clavel's Delta Robot motors. As shown in Fig. 8 paragraph 2.6, 6 moving platform positions are defined to determine the maximum load position of Clavel's Delta Robot. The results of the dynamic simulations show that the maximum motor torque is at position P5. Figs. 11-12 shows the results of dynamic simulation at position P5.

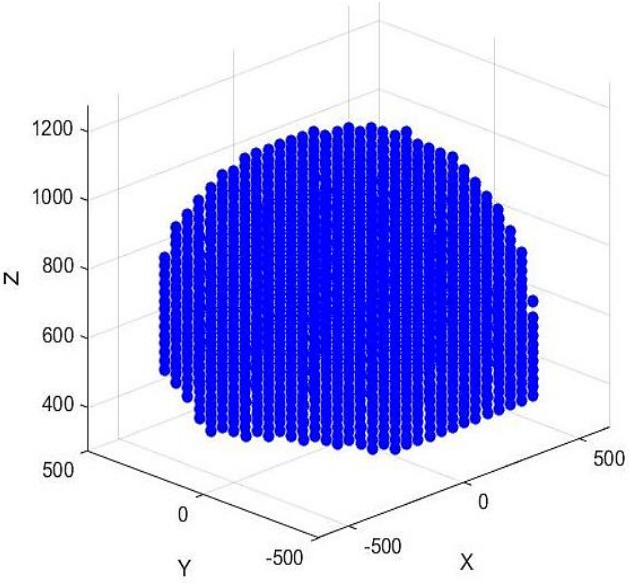

Fig. 10 Workspace according to the inverse problem of kinematics.

In the work of Nadia Cretescu and the authors, a delta robot with spherical joints was studied, where the gap is 0.1 mm, which significantly affects the acceleration of the critical positions and the acceleration changes were 3 times greater than in other positions.[97] In our case, the design features of Clavel's delta robot having rotational connections eliminate the acceleration jump at the critical point (Fig. 11). Fig. 11 shows graphs of changes in generalized coordinates (in degrees), angular velocities (in radians per second), and angular accelerations (in radians per square second), and Fig. 12 also shows the values of generalized forces (moments, in

 © Engineered Science Publisher LLC 2024

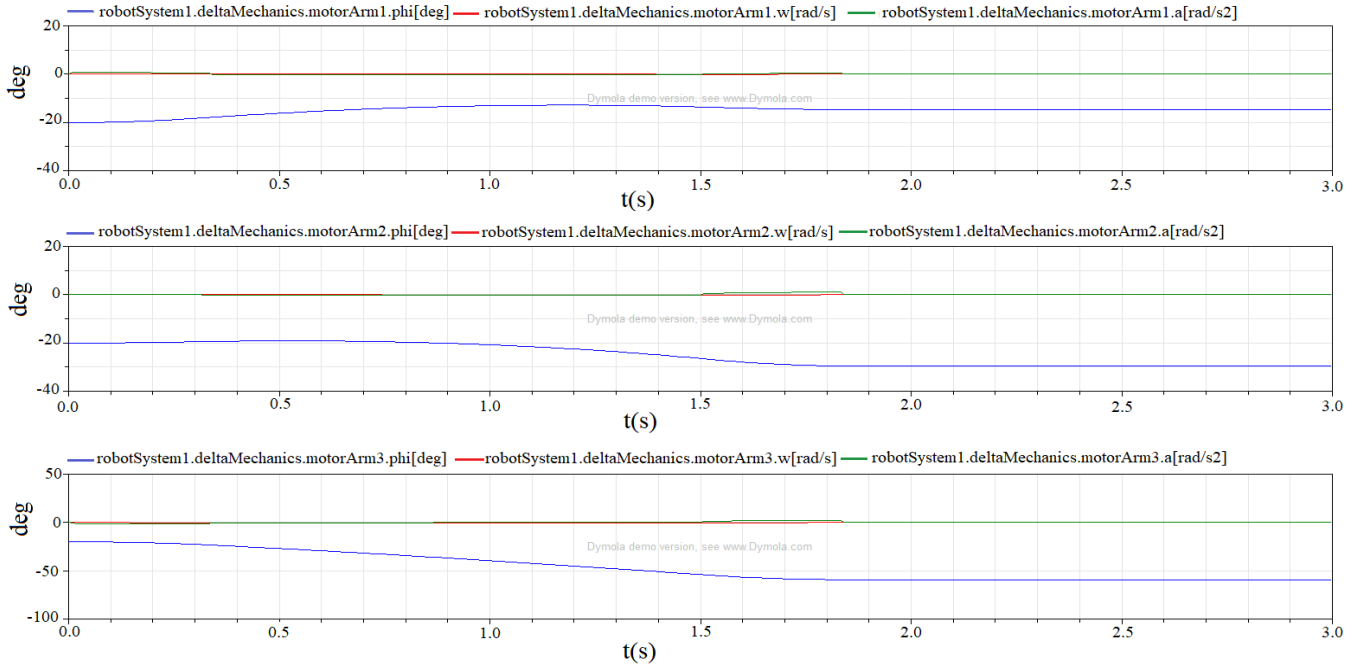

Fig. 11 Velocity and acceleration are angles of rotation of the motor flanges.

newton's per meter) which are determined when moving from position P1 to position P5 (Fig. 8) along the shortest distance. The results of dynamic analysis using the OpenModelica software were verified in the case of equilibrium. As it is known, the partial derivative of the total potential energy of the entire system equals the generalized force, *i.e.*, the torque $\tau_i = \frac{\partial P}{\partial \theta_i} (i = 1, 2, 3)$. Using forward and inverse kinematics, the total potential energy $P(\theta_i)$ of the parallel robot was determined, as well as the torques τ_i acting on the motors at equilibrium. The results obtained from OpenModelica software and the analytical method coincide.

After determining the maximum loaded position (position 5) of Clavel's delta robot, we find the geometric parameters of the legs using cross-section methods. Further, after determining the geometric parameters of the links, the parameters of Clavel's delta robot links in the 3D model are changed and a new value of the mass of the links is obtained. With these values, the calculation is repeated 2 times to get a reliable result. Velocity and acceleration are angles of rotation of the motor flanges in position P5 are not critical (Fig. 11). Based on the results of the dynamic simulation for position P5, the maximum torque in the motor was determined to be 150 Nm (Fig. 12).

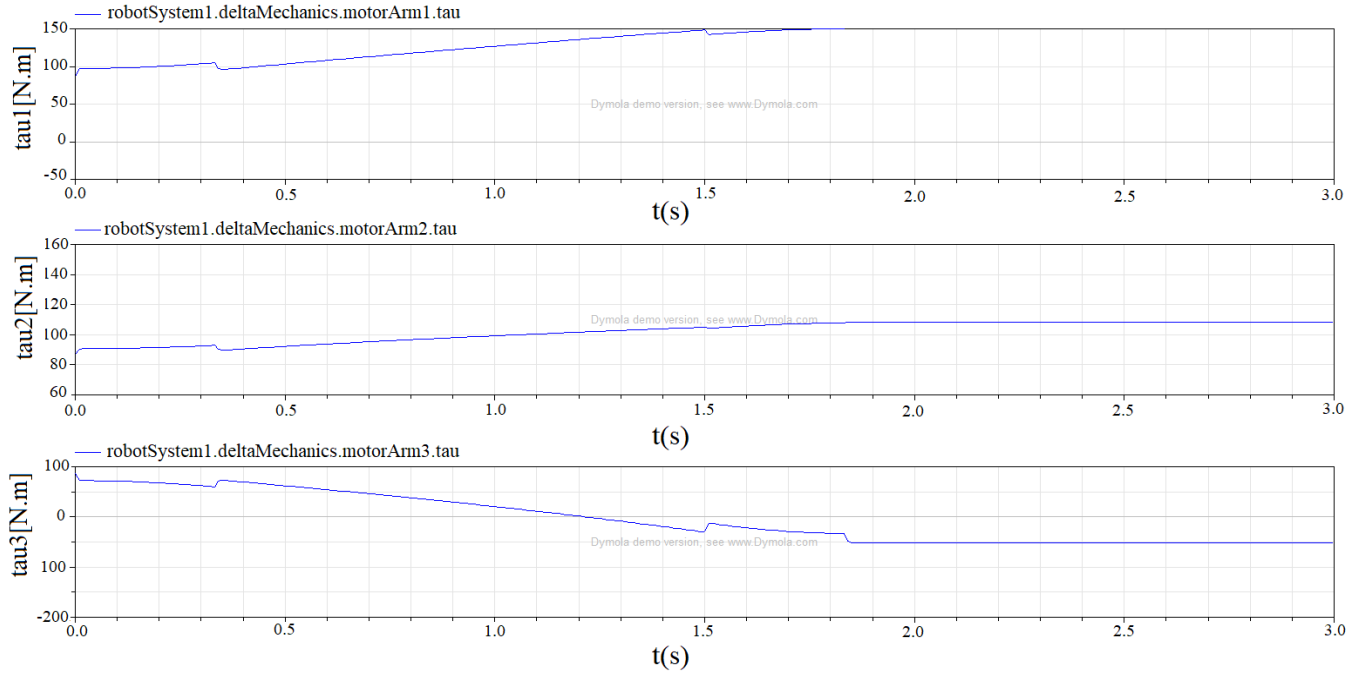

Fig. 12 Torque in the motor flanges.

4. Conclusion

In conclusion, this research paper presents a comprehensive process for selecting a suitable compensating manipulator to improve the positioning accuracy of a printhead mounted on a truck-mounted concrete pump. The operating parameters of the compensating manipulator for compensating the deflections of the truck-mounted concrete pump boom are determined, and a literature review is conducted to determine the most suitable manipulator considering DOF, leg design, and workspace. To determine the workspace and dimensions of 3UPU, 3RUU, Clavel's delta robot, and Electrical Arm manipulators, inverse kinematics problems were solved and the manipulator's workspace and dimensions were determined using MatLab software. Clavel's delta robot was selected based on the requirements and kinematic analysis of various manipulators. The forward and inverse kinematics problems were solved and dynamic simulations were carried out in OpenModelica software to understand and predict the behavior of Clavel's delta robot. The results show that Clavel's delta robot is suitable for use as a manipulator compensating deviations of the printhead installed on the truck-mounted concrete pump from a given trajectory.

The results of the study are a logical continuation of the previous works, where the problem of adapting the truck-mounted concrete pump[34,35] to 3D printing of concrete was solved, but in these works the problem of accuracy of positioning of the printhead was not solved. This scientific work, solving the problem of positioning accuracy of the printhead installed on a truck-mounted concrete pump, is the next step in introducing 3D concrete printing for construction at the lowest cost. If we take into account the fact that a 3D printing mixture of concrete with large gravels (16 mm) has already been developed, which in composition and mechanical characteristics is as close as possible to traditional concrete,[98] and this composition can also be produced and transported by existing construction equipment without changing construction technology. Then, by solving the problem of accurate positioning of the printhead installed on a truck-mounted concrete pump, the barrier that hinders the introduction of 3D concrete printing to the construction industry is removed.

A continuation of this work will be the production of a prototype of Clavel's delta robot and installation of it on a truck-mounted concrete pump for testing in real large-scale construction, where it will be possible to prove the viability of the concepts in practice.

Acknowledgements

This work is supported by the grant "AP19679899 - Research and development of a manipulator that compensating deviations of a construction 3D printer based on a concrete pump truck and positioning the PrintHead" (2023-2025) of the Ministry of Education and Science Kazakhstan.

Conflict of interest

There are no conflicts to declare.

Supporting Information

Not applicable.

References

[1] DIN EN ISO/ASTM 52900: Additive Fertigung—Grundlagen—Terminologie; Beuth Verlag GmbH: Berlin, Germany, 2018.

[2] S. H. Khajavi, M. Tetik, A. Mohite, A. Peltokorpi, M. Li, Y. Weng, J. Holmström, Additive manufacturing in the construction industry: the comparative competitiveness of 3D concrete printing, *Applied Sciences*, 2021, **11**, 3865, doi: 10.3390/app11093865.

[3] B. García de Soto, I. Agustí-Juan, J. Hunhevicz, S. Joss, K. Graser, G. Habert, B. T. Adey, Productivity of digital fabrication in construction: cost and time analysis of a robotically built wall, *Automation in Construction*, 2018, **92**, 297-311, doi: 10.1016/j.autcon.2018.04.004.

[4] A. L. Mohd Tobi, S. A. Omar, Z. Yehia, S. Al-Ojaili, A. Hashim, O. Orhan, Cost viability of 3D printed house in UK, *IOP Conference Series*: *Materials Science and Engineering*, 2018, **319**, 012061, doi: 10.1088/1757-899x/319/1/012061.

[5] J. Otto, J. Kortmann, M. Krause, Wirtschaftliche perspektiven von beton-3D-druckverfahren, *Beton- Und Stahlbetonbau*, 2020, **115**, 586-597, doi: 10.1002/best.201900087.

[6] H. Abdalla, K. P. Fattah, M. Abdallah, A. K. Tamimi, Environmental footprint and economics of a full-scale 3D-printed house, *Sustainability*, 2021, **13**, 11978, doi: 10.3390/su132111978.

[7] Y. Han, Z. Yang, T. Ding, J. Xiao, Environmental and economic assessment on 3D printed buildings with recycled concrete, *Journal of Cleaner Production*, 2021, **278**, 123884, doi: 10.1016/j.jclepro.2020.123884.

[8] J. Wolf, K. T. Werkle, H. C. Möhring, Study on Dynamic Behaviour in FFF 3D-printing with Crossed Gantry Kinematic. *Procedia CIRP*, 2024, **121**, 162-167, doi: 10.1016/j.procir.2023.09.244.

[9] A. Javed, I.M. Mantawy, A. Azizinamini, 3D-Printing of Ultra-High-Performance Concrete for Robotic Bridge Construction, *Journal of the Transportation Research Board*, 2021, **2675,** 307-319, doi:10.1177/03611981211011645

[10] A. Agnihotri, S. Bhattacharya, 3D-Printed Houses: Is Icon Disrupting the Housing Construction Market? *SAGE Publications: SAGE Business Cases Originals*, 2023.

[11] D. Re, C. Di Biccari, A. Corallo, A Cost Model for Additive Manufacturing in Construction, *IOP Conference Series: Earth and Environmental Science*, 2022, **1101**, p. 092014, doi:10.1088/1755-1315/1101/9/092014.

[12] L. D. Evjemo, S. Moe, J. T. Gravdahl, O. Roulet-Dubonnet, L. T. Gellein, Additive manufacturing by robot manipulator: An overview of the state-of-the-art and proof-of-concept results, *2017 22nd IEEE International Conference on Emerging*

 © Engineered Science Publisher LLC 2024

Technologies and Factory Automation, 2017, 1-8, doi:10.1109/ETFA.2017.8247617.

[13] A. Puzatova, P. Shakor, V. Laghi, M. Dmitrieva, Large-scale 3D printing for construction application by means of robotic arm and gantry 3D printer: a review, *Buildings*, 2022, **12**, 2023, doi: 10.3390/buildings12112023.

[14] F. Bos, R. Wolfs, Z. Ahmed, T. Salet, Additive manufacturing of concrete in construction: potentials and challenges of 3D concrete printing, *Virtual and Physical Prototyping*, 2016, **11**, 209–225, doi: 10.1080/17452759.2016.1209867.

[15] Md. Hazrat Ali, Y. Kuralbay, A. Aitmaganbet, M.A.S. Kamal, Design of a 6-DOF robot manipulator for 3D printed construction, *Materials Today: Proceedings*, 2022, **49**, 1462-1468, doi: 10.1016/j.matpr.2021.07.228.

[16] M.E. Tiryaki, X. Zhang, Q.C. Pham, Printing-while-moving: a new paradigm for large-scale robotic 3D Printing, 2019 *IEEE/RSJ International Conference on Intelligent Robots and Systems*, 2019, 2286-2291, doi:10.1109/IROS40897.2019.8967524.

[17] S. Huang, W. Xu, Y. Li, The impacts of fabrication systems on 3D concrete printing building forms. *Frontiers of Architectural research*, 2022, ***11***, 653-669, doi: 10.1016/j.foar.2022.03.004.

[18] C. Gosselin, R. Duballet, P. Roux, N. Gaudillière, J. Dirrenberger, P. Morel, Large-scale 3D printing of ultra-high performance concrete – a new processing route for architects and builders. *Materials & Design*, 2016, **100**, 102–109, doi: 10.1016/j.matdes.2016.03.097.

[19] X. Zhang, M. Li, J.H. Lim, Y. Weng, Y.W.D. Tay, H. Pham, Q.C. Pham, Large-scale 3D printing by a team of mobile robots, *Automation in Construction*, 2018, **95**, 98-106, doi: 10.1016/j.autcon.2018.08.004.

[20] J.-B. Izard, A. Dubor, P.-E. Hervé, E. Cabay, D. Culla, M. Rodriguez, M. Barrado, Large-scale 3D printing with cable-driven parallel robots, *Construction Robotics*, 2017, **1**, 69-76, doi: 10.1007/s41693-017-0008-0.

[21] M. Wehr, Synthetische Faserseile unter hochdynamischer Beanspruchung, *Logistics Journal: Proceedings*, 2017, **10**, 2017, doi: 10.2195/lj_Proc_wehr_de_201710_01.

[22] V. Mechtcherine, V. N. Nerella, F. Will, M. Näther, J. Otto, M. Krause, Large-scale digital concrete construction–CONPrint3D concept for on-site, monolithic 3D-printing, *Automation in Construction*, 2019, **107**, 102933, doi: 10.1016/j.autcon.2019.102933.

[23] M. Krause, J. Otto, A. Bulgakov, D. Sayfeddine, Strategic optimization of 3D concrete printing using the method of CONPrint3D, *Proceedings of the International Symposium on Automation and Robotics in Construction*, 2017, **35**, 1-7, doi:10.22260/isarc2018/0002.

[24] A. Badr, C. Fentiman, M. Grantham, R. Mangabhai, Concrete for the Modern Age Developments in materials and processes, Whittles Publishing. 2017.

[25] R. Liu, Y. Gao, S. Yang, Y. Yang, Vibration control of the boom system of truck-mounted concrete pump based on constant-position commandless input shaping technique, *Shock and Vibration*, 2015, **2015**, 420935, doi: 10.1155/2015/420935.

[26] W. Yang, B. Zhang, Y. Huang, Q. Cai, P. Zhang, Rotary vibration control simulation and experiment research on the boom of concrete pump truck, 2017 IEEE 3rd Information Technology and Mechatronics Engineering Conference, 2017.

[27] Y. Huang, B.-X. Wu, J.-Q. Wang, Test for active control of boom vibration of a concrete pump truck, *Journal of Vibration and Shock*, 2012, **31**, 91–94.

[28] F. Resta, F. Ripamonti, G. Cazzulani, M. Ferrari, Independent modal control for nonlinear flexible structures: an experimental test rig, *Journal of Sound and Vibration*, 2010, **329**, 961-972, doi: 10.1016/j.jsv.2009.10.021.

[29] G. Cazzulani, F. Resta, F. Ripamonti, A feedback and feedforward vibration control for a concrete placing boom, *Journal of Vibration and Acoustics*, 2011, **133**, 051002, doi: 10.1115/1.4003932.

[30] G. Bagordo, G. Cazzulani, F. Resta, F. Ripamonti, A modal disturbance estimator for vibration suppression in nonlinear flexible structures, *Journal of Sound and Vibration*, 2011, **330**, 6061-6069, doi: 10.1016/j.jsv.2011.07.014.

[31] R. Ding, J. Wang, M. Cheng, X. Luo, B. Xu, Vibration-polynomial-based optimal trajectory planning for mobile concrete pumping equipment with state constraints, *Automation in Construction*, 2024, **158**, 105246, doi: 10.1016/j.autcon.2023.105246.

[32] X. Sun, H. Ye, S. Fei, A closed-loop detection and open-loop control strategy for booms of truck-mounted concrete pump, *Automation in Construction*, 2013, **31**, 265-273, doi: 10.1016/j.autcon.2012.12.012.

[33] G. Cazzulani, C. Ghielmetti, H. Giberti, F. Resta, F. Ripamonti, Overview on the truck mounted concrete boom pump: a dynamic numerical model for active control logic definition, *IFAC Proceedings Volumes*, 2011, **44**, 4232-4237, doi: 10.3182/20110828-6-it-1002.02072.

[34] S. Zorn, F. Will, P. Mögle, Control stabilization of multilink manipulators in a truck-mounted concrete boom pump, *ATZoffhighway Worldwide*, 2018, **11**, 44-49, doi: 10.1007/s41321-018-0026-y.

[35] Digitalies Bauen - Großformatiger 3D-Druck mit Transportbeton (ready2print), 2023.

[36] F. Storch, Beton-3D-Druck - Neues Anwendungsfeld für Autobetonpumpen, Tagungsband Praxis Transportbeton, Berlin, 2022.

[37] Beton-3D-Druck-Machbarkeitsuntersuchungen zu kontinuierlichen und schalungsfreien Bauverfahren durch 3D-Formung von Frischbeton, Final report Dresden, 2016.

[38] F. Storch, P. Plaschnick, F. Will, CONPrint3D-Aktuelle Entwicklungsschwerpunkte beim Beton-3D-Druck, Tagungsband 9. Fachtagung Baumaschinentechnik, 2022.

[39] S. Zorn, F. Will, P. Mögle, Regelungstechnische Stabilisierung mehrgliedriger Ausleger bei einer Autobetonpumpe, *ATZoffhighway*, 2018, ***11***, 46-51, doi: 10.1007/s35746-018-0026-y.

© Engineered Science Publisher LLC 2024

[40] Digitales Bauen – Großformatiger 3D-Druck mit Transportbeton, 2023.
[41] Modellbasierte aktive Schwingungstilgung eines MultilinkGroßraummanipulators, Dissertation Technischen Universität Dresden, 2017.
[42] S. Zorn, F. Will, P. Mögle, Control stabilization of multilink manipulators in a truck-mounted concrete boom pump, *ATZoffhighway Worldwide*, 2018, **11**, 44-49, doi: 10.1007/s41321-018-0026-y.
[43] K.M. Lynch, F.C. Park, Modern robotics, *Cambridge University Press*, 2017, doi:10.1017/9781316661239.
[44] J.P. Merlet, Parallel Robots, *Springer Science & Business Media*, 2005, **128**, doi:10.1007/1-4020-4133-0.
[45] J. Kirchner, Mehrkriterielle Optimierung von Parallelkinematiken, Berichte aus dem Fraunhofer IWU, 2001.
[46] B. Dasgupta, T. S. Mruthyunjaya, The Stewart platform manipulator: a review, *Mechanism and Machine Theory*, 2000, **35**, 15-40, doi: 10.1016/s0094-114x(99)00006-3.
[47] R. Neugebauer, Parallel kinematische Maschinen: Entwurf, Konstruktion, Anwendung. Berlin, Heidelberg: Springer Berlin Heidelberg, 2006.
[48] M. Uchiyama, Structures and characteristics of parallel manipulators, *Advanced Robotics*, 1993, **8**, 545-557, doi: 10.1163/156855394x00248.
[49] S. Hesse, V. Malisa, A. Almansa, R. Ambrosch, B. Graf, C. Hieger, M. Trenker, W. Kubinger, Taschenbuch Robotik-Montage-Handhabung, *Aufl. München: Carl Hanser*, 2010.
[50] A. A. Shaik, N. S. Tlale, G. Bright, A new hybrid machine design for a 6 DOF industrial robot arm, *International Journal of Intelligent Systems Technologies and Applications*, 2012, **11**, 63, doi: 10.1504/ijista.2012.046544.
[51] L. Sun, L. Fang, An approximation method for stiffness calculation of robotic arms with hybrid open- and closed-loop kinematic chains, *Advances in Mechanical Engineering*, 2018, **10**, 168781401876129, doi: 10.1177/1687814018761297.
[52] S. Kumar, H. Wöhrle, J. de Gea Fernández, A. Müller, F. Kirchner, A survey on modularity and distributivity in series-parallel hybrid robots, *Mechatronics*, 2020, **68**, 102367, doi: 10.1016/j.mechatronics.2020.102367.
[53] J. P. Merlet, Parallel robots. *Springer Science & Business Media*, 2005.
[54] M. Badescu, C. Mavroidis, Workspace optimization of 3-legged UPU and UPS parallel platforms with joint constraints, *Journal of Mechanical Design*, 2004, **126**, 291-300, doi: 10.1115/1.1667922.
[55] K.A.A. Ali, Y. Liu, Position Analysis of 3-DOF 3-RPS Parallel Manipulator, *Proceedings of the 2016 International Conference on Advanced Materials Science and Environmental Engineering,* 2016, 126-129, doi: 10.2991/amsee-16.2016.35.
[56] J.W. Park, W. Jeon, Y.K. Kang, H.S. Yang, H. Park, Instantaneous kinematic analysis for a crawler type in-pipe robot, *IEEE International Conference on Mechatronics, IEEE*, 2011, 381-385, doi: 10.1109/ICMECH.2011.5971315.
[57] P. Babu, R. Sivaramakrishnan, Simulation and singularity analysis of 3-PRS parallel manipulator, *IEEE International Conference on Mechatronics and Automation. IEEE,* 2012, 2203-2207, doi: 10.1109/ICMA.2012.6285685.
[58] C. Dhandapani, R. Sivaramakrishnan, G. Gayaz, R. Govindraj, Modelling and analysis of A 3-dof triglide parallel manipulator with extensible links for angular drilling operations, *Mechanical Engineering,* 2020, **8**, doi: 10.17577/IJERTCONV8IS06025.
[59] D. Glozman, M. Shoham, Novel 6-DOF parallel manipulator with large workspace, *Robotica*, 2009, **27**, 891-895, doi: 10.1017/s0263574708005286.
[60] H. Zohoor, M. Vakil, H. Pendar, On the Kinematic Analysis of a Spatial Six-Degree-of-Freedom Parallel Manipulator, Scientia Iranica, 2009.
[61] M. H. Abedinnasab, F. Farahmand, B. Tarvirdizadeh, H. Zohoor, J. Gallardo-Alvarado, Kinematic effects of number of legs in 6-DOF UPS parallel mechanisms, *Robotica*, 2017, **35**, 2257-2277, doi: 10.1017/s0263574716000862.
[62] L.W. Tsai, Kinematics of A three-DOF platform with three extensible limbs. *Advances in Robot Kinematics. Dordrecht: Springer,* 1996, 401-410, doi:10.1007/978-94-009-1718-7_40.
[63] A. Hassani, S. A. Khalilpour, A. Bataleblu, H. D. Taghirad, Full dynamic model of 3-UPU translational parallel manipulator for model-based control schemes, *Robotica*, 2022, **40**, 2815-2830, doi: 10.1017/s0263574721001971.
[64] J. Bałchanowski, Positioning accuracy analysis of the parallel mechanism near singular positions, *International Journal of Applied Mechanics and Engineering*, 2015, **20**, 5-18, doi: 10.1515/ijame-2015-0001.
[65] Y. Li, Q. Xu, Stiffness analysis for a 3-PUU parallel kinematic machine, *Mechanism and Machine Theory*, 2008, **43**, 186-200, doi: 10.1016/j.mechmachtheory.2007.02.002.
[66] M. Maya, E. Castillo, A. Lomelí, E. González-Galván, A. Cárdenas, Workspace and payload-capacity of a new reconfigurable delta parallel robot, *International Journal of Advanced Robotic Systems*, 2013, **10**, 56, doi: 10.5772/54670.
[67] M. A. Laribi, L. Romdhane, S. Zeghloul, Analysis and dimensional synthesis of the DELTA robot for a prescribed workspace, *Mechanism and Machine Theory*, 2007, **42**, 859-870, doi: 10.1016/j.mechmachtheory.2006.06.012.
[68] X.-J. Liu, J. Wang, K.-K. Oh, J. Kim, A new approach to the design of a DELTA robot with a desired workspace, *Journal of Intelligent and Robotic Systems*, 2004, **39**, 209-225, doi: 10.1023/B: JINT.0000015403.67717.68.
[69] L. Scalera, P. Boscariol, G. Carabin, R. Vidoni, A. Gasparetto, Enhancing energy efficiency of a 4-DOF parallel robot through task-related analysis. *Machines*, 2020, ***8***, 10, doi:10.3390/machines8010010.
[70] B. Lian, L. Wang, X. V. Wang, Elastodynamic modeling and parameter sensitivity analysis of a parallel manipulator with articulated traveling plate, *The International Journal of Advanced Manufacturing Technology*, 2019, **102**, 1583-1599, doi: 10.1007/s00170-018-03257-x.

 © Engineered Science Publisher LLC 2024

[71] M. Solazzi, M. Gabardi, A. Frisoli, M. Bergamasco, Kinematics analysis and singularity loci of a 4-UPU parallel manipulator, *Advances in Robot Kinematics*, 2014, 467-474, doi:10.1007/978-3-319-06698-1_48.
[72] T. S. Zhao, Y. W. Li, J. Chen, J. C. Wang, A novel four-DOF parallel manipulator mechanism and its kinematics, 2006 *IEEE Conference on Robotics, Automation and Mechatronics*, 2006, 1-5, doi:10.1109/RAMECH.2006.252672.
[73] M. H. Abedinnasab, G. R. Vossoughi, Analysis of a 6-DOF redundantly actuated 4-legged parallel mechanism, *Nonlinear Dynamics*, 2009, **58**, 611-622, doi: 10.1007/s11071-009-9504-1.
[74] B.-J. Yi, D. Cox, D. Tesar, Analysis and design criteria for a redundantly actuated 4-legged six degree-of-freedom parallel manipulator, *IEEE International Conference on Robotics and Automation,* 2001, **4,** 3286-3293, doi: 10.1109/ROBOT.2001.933125.
[75] G. Cui, H. Zhang, F. Xu, C. Sun, Kinematics dexterity analysis and optimization of 4-UPS-UPU parallel robot manipulator, *Intelligent Robotics and Applications: 7th International Conference,* 2014, 1-11, doi:10.1007/978-3-319-13963-0_1.
[76] D. Stewart, A platform with six degrees of freedom, *Proceedings of the Institution of Mechanical Engineers*, 1965, **180**, 371-386, doi: 10.1243/pime_proc_1965_180_029_02.
[77] L.W. Tsai, Robot analysis: the mechanics of serial and parallel manipulators. John Wiley & Sons, Inc., New York/Singapore/Toronto, 1999.
[78] B. Dasgupta, T. S. Mruthyunjaya, The Stewart platform manipulator: a review, *Mechanism and Machine Theory*, 2000, **35**, 15-40, doi: 10.1016/s0094-114x(99)00006-3.
[79] M.S. Narayanan, S. Chakravarty, H. Shah, V.N. Krovi, Kinematic, static and workspace analysis of a 6-P-U-S parallel manipulator, *International Design Engineering Technical Conferences and Computers and Information in Engineering Conference*, 2010, **44106**, 1456-1456, doi: 10.1115/DETC2010-28978.
[80] X. Liu, Y. Xu, J. Yao, J. Xu, S. Wen, Y. Zhao, Control-faced dynamics with deformation compatibility for a 5-DOF active over-constrained spatial parallel manipulator 6PUS–UPU, *Mechatronics*, 2015, **30**, 107-115, doi: 10.1016/j.mechatronics.2015.06.014.
[81] E. Mirshekari, A. Ghanbarzadeh, K. H. Shirazia, Structure comparison and optimal design of 6-RUS parallel manipulator based on kinematic and dynamic performances, *Latin American Journal of Solids and Structures*, 2016, **13**, 2414-2438, doi: 10.1590/1679-78252937.
[82] J. Aginaga, I. Zabalza, O. Altuzarra, J. Nájera, Improving static stiffness of the 6-RUS parallel manipulator using inverse singularities, *Robotics and Computer-Integrated Manufacturing*, 2012, **28**, 458-471, doi: 10.1016/j.rcim.2012.02.003.
[83] J. Niu, H. Wang, Z. Jiang, L. Chen, J. Zhang, Y. Feng, S. Guo, Kinematic analysis of a serial-parallel hybrid mechanism and its application to a wheel-legged robot, *IEEE Access*, 2020, **8**, 111931-111944, doi: 10.1109/ACCESS.2020.3001653.
[84] S. D. Monk, A. Grievson, M. Bandala, C. West, A. Montazeri, C. J. Taylor, Implementation and evaluation of a semi-autonomous hydraulic dual manipulator for cutting pipework in radiologically active environments, *Robotics*, 2021, **10**, 62, doi: 10.3390/robotics10020062.
[85] B. Tidå, Seeking the spotlight: How reputational considerations shape the European Court of Auditor's shifting account-holding role, *Public Administration*, 2022, **100**, 692-710, doi: 10.1111/padm.12766.
[86] H. A. Rana, S. Kapil, Redundantly Actuated Hybrid Kinematic setup for high Manipulability Advances In Robotics, *6th International Conference of The Robotics Society*, 2023, 1-10, doi: 10.1145/3610419.3610475.
[87] M. Elsamanty, E. M. Faidallah, Y. H. Hossameldin, S. A. Rabbo, S. A. Maged, H. Yang, K. Guo, Workspace analysis and path planning of a novel robot configuration with a 9-DOF serial-parallel hybrid manipulator (SPHM), *Applied Sciences*, 2023, **13**, 2088, doi: 10.3390/app13042088.
[88] I. Ben Hamida, M. A. Laribi, A. Mlika, L. Romdhane, S. Zeghloul, Dimensional synthesis and performance evaluation of four translational parallel manipulators, *Robotica*, 2021, **39**, 233-249, doi: 10.1017/s026357472000034x.
[89] L.W. Tsai, Robot analysis: the mechanics of serial and parallel manipulators. New York John Wiley & Sons, 1999.
[90] T. Zar, P. Wai Lin, D. S. Yin Win, Workspace analysis of two-link planar manipulator, *International Journal of Science and Engineering Applications*, 2019, **8**, 380-383, doi: 10.7753/ijsea0808.1028.
[91] T. Bentaleb, H. Hammache, B.M. El Amine, Workspace, Accuracy Analysis and Kinematic Calibration of a" Delta" Parallel Robots, In Proceedings of the International Conference on Electronics & Oil: From theory to applications, 2011.
[92] C. Woernle, C. Woernle, (Hrsg.): Mehrkörpersysteme. 2. Aufl. Berlin, Heidelberg: Springer, 2016.
[93] P. Campanini, G. Ferretti, Object-Oriented Models of Parallel Manipulators, *Proceedings of 14th Modelica Conference*, 2021, 241-248, doi:10.3384/ecp21181241.
[94] K. Miller, Proceedings of 1995 IEEE International Conference on Robotics and Automation, *Proceedings of 1995 IEEE International Conference on Robotics and Automation*, 1995, 532-537, doi: 10.1109/robot.1995.525251.
[95] R. Clavel, A fast robot with parallel geometry, In Proc. of the Int. Symp. on Industrial Robot, Switzerland, 1988, **26-28**, 91-100.
[96] L. Rey, R. Clavel, The delta parallel robot. Parallel Kinematic Machines. *London: Springer London,* 1999, 401-417, doi: 10.1007/978-1-4471-0885-6_29.
[97] N. Cretescu, M. Neagoe, R. Saulescu, Dynamic analysis of a delta parallel robot with flexible links and joint clearances, *Applied Sciences*, 2023, **13**, 6693, doi: 10.3390/app13116693.
[98] M. Taubert, V. Mechtcherine, Mix design for a 3D-

printable concrete with coarse aggregates and consideration of standardization, RILEM International Conference on Concrete and Digital Fabrication. Cham: Springer, 2022.

Publisher's Note: Engineered Science Publisher remains neutral with regard to jurisdictional claims in published maps and institutional affiliations.

© Engineered Science Publisher LLC 2024